Materials Science and Engineering C 70 (2017) 303–310

Contents lists available at ScienceDirect

Materials Science and Engineering C

journal homepage: www.elsevier.com/locate/msec

Effects of halloysite nanotubes on physical properties and cytocompatibility of alginate composite hydrogels

Biao Huang, Mingxian Liu *, Zheru Long, Yan Shen, Changren Zhou *

Department of Materials Science and Engineering, Jinan University, Guangzhou 510632, China

ARTICLE INFO

Article history:
Received 18 July 2016
Received in revised form 10 August 2016
Accepted 1 September 2016
Available online 02 September 2016

Keywords:
Halloysite
Alginate
Hydrogels
Biocompatibility
Bone tissue engineering

ABSTRACT

Sodium alginate (SA)/halloysite nanotubes (HNTs) composite hydrogels were successfully prepared by solution blending and cross-linking with calcium ions. HNTs can improve the physical properties and cytocompatibility of composite hydrogels. The static and shear viscosity of SA/HNTs solution increase by the addition of HNTs. FTIR suggests the presence of hydrogen bond interactions between HNTs and SA. The crystal structure of HNTs is retained in the composites as showed by the X-ray diffraction result. A porous structure with pore size of 100–250 μm is found in the hydrogels, which can provide a space for cell growth and migration. The compressive mechanical properties of composite hydrogels significantly increase compared to the pure SA hydrogel. The SA/HNTs composite hydrogels with 80% HNTs loading exhibit the compressive stress at 80% strain of 2.99 MPa, while the stress at 80% strain of pure SA hydrogel is only 0.8 MPa. The dynamic storage modulus of composite hydrogels also markedly increases with HNTs concentration. The differential scanning calorimetry endothermic peak area and swelling ratios in NaCl solution of the composite hydrogels decrease by the addition of HNTs. Preosteoblast (MC3T3-E1) culture results reveal that the SA/HNTs composites especially at relatively low HNTs loading show a significant increase in cells adhesion and proliferation compared to the pure SA hydrogel. All the results demonstrate that the SA/HNTs composite hydrogels show a promising application in bone tissue engineering.

1. Introduction

Tissue engineering is considered as a potentially valuable method to repair the tissue defects by autologous cells/tissue transplantation technology [1]. Porous degradable scaffolds provide a specific environment for cells/tissue growth in vivo and vitro. Many types of materials, including polymers, inorganics, and metals, have been applied to fabricate tissue engineering scaffolds [2–4]. Recently, composite scaffolds which are a combination of the different advantage materials have been designed to satisfy the rigorous need for tissue growth. For ideal tissue engineering scaffolds, they should have sufficient porosity, interconnection channels employed to transport nutrients, well biocompatibility and biodegradability, as well as with a high mechanical strength [5]. Among the materials used for tissue engineering scaffolds, synthetic biodegradable polymers represent an important type since their properties can be readily adjusted via the control of the polymerization reaction [6]. The main drawback of the synthetic biodegradable polymer scaffolds is lack of the bioactivity. Biomacromolecules (such as protein, nucleic acid or polysaccharide) derived from natural resource is another type of scaffold materials. They have many advantages in the application of biomedical areas, such as fine biodegradable, biocompatible, antithrombotic (prevents blood clots) and hemostatic properties, remarkable healing activity, water retention capacity, antibacterial, immunological and anti-tumor properties, and low cost [7–9].

Alginic acid is a natural polysaccharide copolymer consisting of β-D-mannuronic acid (M units) and α-L-guluronic acid (G units) [10], which has widespread application in biomedical areas. Sodium alginate (SA) can form a gel rapidly in the presence of divalent metal ions by the complexation. The SA hydrogels have been extensively applied in drug/gene delivery, tissue engineering, wound healing, cell encapsulation, and so on [11,12]. SA hydrogel as scaffold for tissue engineering has unique advantages, for example, they can be mixed with the cells in liquid form into the body to fill the damaged tissue, the three-dimensional network structure is similar to skeleton to provide a three-dimensional growing space for cells growth [13,14]. Owing to the high rate of degradation in cell culture and the weak mechanical properties, a single component SA hydrogel limits the practical application. To solve this issue, SA has been combined with various components to obtain different composite scaffolds. The nanosilica, α/β-tricalcium phosphate, graphene oxide (GO), halloysite nanotubes (HNTs), and chitin whisker, have been incorporated into alginate matrix which is aiming to improve the adsorption efficient, mechanical strength, and other physical properties [15–18]. For example, the addition of GO can greatly increase the thermal stability and mechanical properties of the SA composite [19,20]. Chitin whiskers can also markedly promote the cell adhesion and proliferation of

* Corresponding authors.
E-mail addresses: liumx@jnu.edu.cn (M. Liu), tcrz9@jnu.edu.cn (C. Zhou).

http://dx.doi.org/10.1016/j.msec.2016.09.001
0928-4931/

osteoblast cells into the SA nanocomposite hydrogels [15]. Our previous work has revealed that HNTs can effectively improve the compressive mechanical properties and cytocompatibility of SA scaffold [21].

Halloysite is a natural mineral nanotube with high aspect ratio and an empty lumen. HNTs have many virtues as polymer nanofiller such as good dispersion properties, numerous active groups on their surfaces, low toxicity, good biocompatibility, and inexpensive [22–26]. They can easily be dispersed in different polymers and shows a good reinforcing ability for the composites [27]. In recent years, HNTs have attracted wide attentions as novel biomaterials. Firstly, HNTs can be used as drug delivery carriers attributed to their unique nanostructure. Anticancer drugs such as curcumin and doxorubicin (DOX), DNA, protein, antibacterial agent have been included in the tubes for slow releasing [28–31]. HNTs-chitosan sponges can also be found with high hemostatic performance and accelerate wound healing process [23]. Recently, HNTs patterned nanosurfaces have been used to capture circulating tumor cells, which can be used as cancer early diagnose [32,33]. HNTs have good interfacial interactions with SA via hydrogen bonding, which can be employed to prepare composite hydrogel beads or porous scaffolds. Wang et al. prepared diclofenac sodium-loaded SA/hydroxyapatite/HNTs nanocomposite hydrogel beads by the method of dropping the solution into a calcium chloride solution. The tubular structure of the HNTs can restrict movability of the SA polymer chains, which is the main reason for the improved drug loading and release behavior [34]. Liu et al. also prepared SA/HNTs beads for removal of dye from aqueous solution, and they found that not only the adsorption capacity of SA/HNT hybrid beads was improved but also the stability in the solution was enhanced significantly [35]. The effect of HNTs on the physical–chemical properties of SA hydrogel beads has also been studied [36]. However, adopting the dropping-precipitation method is notoriously difficult to prepare large size and size-controllable SA hydrogel. The hydrogel beads cannot satisfy the requirement of tissue engineering scaffold.

In this work, columnar composite hydrogel composed with HNTs and SA solution was prepared by casting the mixture solution in a mold and then cross-linking with $CaCl_2$ solution method. The influences of the addition of HNTs on the solution viscosity, dimensional stability, mechanical properties, pore structure, and cell attachment of SA are investigated. The results show that the compressive strength, structural stability, and biocompatibility of SA/HNTs composite hydrogel improved, which contribute to the potential application of SA/HNTs composite hydrogel in bone tissue engineering.

2. Experimental

2.1. Materials

Alginic acid sodium salt from brown algae (SA) (medium viscosity, ≥2000 cP, 2%(25 °C)) was purchased from Sigma-Aldrich (Shanghai, China). Halloysite nanotubes (HNTs), with molecular formula of $Al_2Si_2O_5(OH)_4 \cdot 2H_2O$, were purchased from Guangzhou Runwo Materials Technology Co., Ltd., China. Ultrapure water from a Milli-Q water system was used in all experiments. Acridine orange (AO), RPMI 1640 medium, fluorescein isothiocyanate isomer I (FITC), and dimethyl sulfoxide (DMSO) were purchased from Nanjing Keygen Biotech Co., Ltd., DAPI (4′,6-diamidino-2-phenylindole) and Phalloidin–Tetramethylrhodamine B isothiocyanate (phalloidin-TRITC) were purchased from Guangzhou Jetway Biotech Co., Ltd. Calcium chloride ($CaCl_2$) and other chemicals reagents were purchased from Aladdin (Shanghai, China) were analytically pure without further purification.

2.2. Preparation of SA/HNTs composite hydrogels

The SA/HNTs composite hydrogels were prepared by the method of solution blending and subsequent cross-linking in calcium ions. The typical procedure was as follows. 1.5, 3, 6, and 12 g HNTs were dispersed separately in ultrapure water (100 mL) by magnetic stirring for 30 mins and ultrasonic at 700 W for 30 min. Subsequently, 3 g of SA powder was added into the solution above, continuously stirred overnight. 2 mL mixed solution was cast in 24-well plastic culture plates with syringe, then the mixed solutions were cross-linked with 5 wt.% $CaCl_2$ solution after 24 h. Afterwards, the hydrogels were removed from the plastic culture plates and kept in ultrapure water at 4 °C. According to the HNTs concentration from low to high, the hydrogels were decoded in turn as SA (prepared with pure SA solution), SA2N1, SA1N1, SA1N2, and SA1N4 (the weight ratio of SA and HNTs was separately 2:1, 1:1, 1:2, 1:4; For example, the 'SA2N1' means the weight ratio of SA and HNTs in the hydrogel was 2:1). Thin hydrogel films for storage modulus test and cell experiment were prepared by casting and paving 1 mL solution on the glass slide immersed in 5% $CaCl_2$ solution. The thickness of the films is about 1 mm.

2.3. Characterization

The Brookfield viscometer (DV2TRVTJ0, Brookfield) was used to determine static viscosity of pure SA and SA/HNTs mixed solutions at a speed of 100 RPM for 1 min at 25 °C. A rotational rheometer (Kinexus pro+, Malvern Instruments, Malvern, UK.) was used to measure the dynamic viscosity of the solutions at room temperature at the shear rate of 1–100 s^{-1}. Compression testing of the wet hydrogels was performed using the Zwick/Roell Z005 machine under 25 °C at a speed of 2 mm/min. The section morphology of the composite hydrogels was analyzed by means of SEM (S-4800 FE, Hitachi) at voltage of 2 kV. Before observation, the wet hydrogels were freeze–dried, sectioned, and sputtered with gold. The pore structure was further visualized by fluorescent microscope (XDY-2, Yuexian optical instruments, Guangzhou, China). Before observation, the wet hydrogel samples were stained by 1 mg/mL FITC aqueous solution and then freeze–dried. X-ray diffraction (XRD) profiles for milled and lyophilized samples were obtained using X-ray diffractometer (D8, Bruker) at room temperature. The scanning angle was from 5° to 60° and a scanning speed of 10°/min with 40 kV voltages and 15 mA current. The powder samples were also analyzed in a FTIR spectrometer (VERTEX 70, Bruker) at room temperature, the

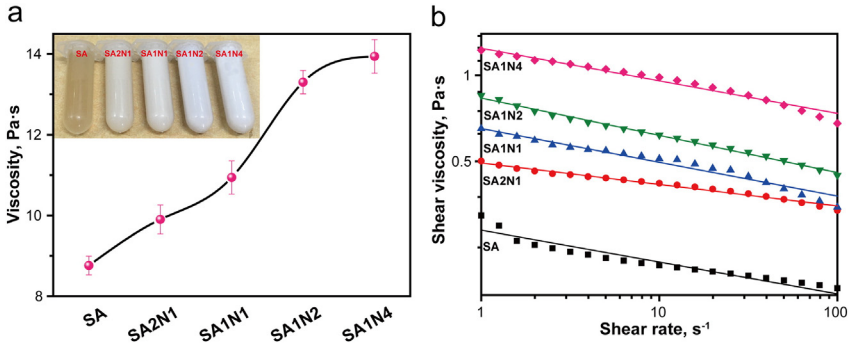

Fig. 1. (a) Static viscosity of pure SA and SA/HNTs solutions; (b) dynamic viscosity of pure SA and SA/HNTs solutions (the solid lines is fitting curve according to power-law equation).

wavelength was changed from 400 cm^{-1} to 4000 cm^{-1}. The change of storage modulus also was analyzed in room temperature with strains sweep (0.1–100%) and frequency scanning (0.1 Hz–100 Hz) for SA and SA/HNTs round hydrogel films with a diameter of 15 mm and a thickness of 1 mm by a rotational rheometer. The strain sweep was carried out at a fixed frequency of 1 Hz and the frequency sweep was carried out at the fixed strain of 0.5%. The thermal properties of the powder samples were also measured in differential scanning calorimetry (DSC) using TA/Q20/DSC instruments. To study the volume change of gels after cross-linked, the shrinkage ratio (SR) was calculated using the formula:

$$SR = \frac{R-r}{R} \times 100\% \quad (1)$$

where, R was the diameter of 24-well plastic culture plates and r was the diameter of wet hydrogels. The equilibrium swelling ratios (ESR) were determined as:

$$ESR = W_s/W_d \quad (2)$$

where, W_s was the weight of the swollen hydrogels in 0.1 M NaCl solution at 37 °C and W_d was the weight of the oven-dried hydrogels. All experiments were repeated over three times [37].

2.4. Cell viability and morphology

The thin hydrogel films were sterilized in autoclaves sterilizers at 120 °C, then were transferred into 24-well plastic culture plates. The MC3T3-E1 cells were cultured in RPMI 1640 Medium, supplemented with 10% fetal bovine serum at 37 °C in 5% CO_2 and 95% air. MC3T3-E1 cells were seeded onto hydrogels slice at a density of 1×10^4 cells/mL, then stained with AO and observed under a fluorescent microscope (XDY-2, Yuexian optical instruments, Guangzhou, China).

Hydrogel samples were soaked in clean water and the soakage liquid was extracted after 48 h. The extract liquid was then added into RPMI 1640 medium with 10% fetal bovine serum at a ratio of 1:2, which as the medium was used to culture MC3T3-E1 cell at 37 °C in 5% CO_2 and 95% air at a density of 1×10^4 cells/mL. MTT colorimetric assay was used to investigate the cell activity in a Microplate System (Thermo, Multiskn MK3, Shanghai, China) at 490 nm.

The confocal laser scanning microscope (CLSM; 510 Meta Duo Scan; Carl Zeiss, Germany) was used to observe the morphology of MC3T3-E1 cells growth on SA, SA2N1, and SA1N1 hydrogels after 3 days (cells were cultured in the same conditions as the previous). The cells were fixed with 4% paraformaldehyde (Macklin, MFCD00133991) and permeated with 0.5% triton-100 (M003798, Micxy reagent). Cells nuclei and skeleton were stained with DAPI and phalloidin-TRITC respectively.

3. Results and discussion

3.1. The viscosity of SA/HNTs solutions

Solution viscosity is an important parameter that affects the fluid flow ability when molding. The polymer solution viscosity is related to solution concentration, polymer molecular weight, filler type and content, and the measure condition. Fig. 1(a) compares the static viscosity of different composite solutions. It can be seen that the solution viscosity gradually increases from 8.7 Pa·s to 13.9 Pa·s by the addition of HNTs. This is ascribed to the thickening effect of HNTs, which is related to the formed HNTs network in the solution. By further loading of HNTs, the solution viscosity is too high to cast into the mold. So, we prepared the composite hydrogels with a maximum HNTs loading of 80 wt.% (SA1N4). From the inset images of Fig. 1(a), the solution turn from clear and translucent of pure SA solution to turbidity and opaque of the mixture solutions. However, even when the loading of HNTs is high, the solution is homogeneous before the preparation of the hydrogels without sedimentation. The dynamic viscosity of the solution was further investigated (Fig. 1(b)). It can be seen the shear viscosity of all the samples decreases with the shear rate. The addition of HNTs also leads to the increase of the viscosity. For example, the shear viscosity of SA1N4 solution changes from 1.63 to 0.68 Pa·s, while the pure SA solution changes from 0.32 to 0.18 Pa·s. The homogeneous SA/HNTs solutions are cast into the cylindrical modulus and cross-linked by $CaCl_2$ overnight to form a uniform hydrogel.

The different rheological behaviors of pure SA and SA/HNTs solutions were further investigated by fitting the data by the power law equation [38,39]:

$$\eta(\gamma) = k\gamma^{(n-1)} \quad (3)$$

where k is the consistency index (Pa·s^n), which is related to the magnitude of the shear viscosity; n is the power law index, ranging between 0 and 1, i.e. it is equal to 1 for Newtonian behavior and decreases with increasing the non-Newtonian behavior. The fitting curves are shown in Fig. 1(b). The power law model parameters k, n, and R^2 were summarized in Table 1. From the curves and the R^2 values ($R^2 \approx 1$), it can be seen that the flow behavior of all the solutions fits well with the power law model. k value increases from 0.2971 to 1.2445 with the HNTs content, which suggests that the solution viscosity increases by the addition of nanotubes. This result is consistent with the previously reported composite systems in which the addition of particles into polymers leaded to an increase of the k value [40,41]. Both pure SA and SA/HNTs solutions are shear thinning and have $n < 1$. The n value of the mixture solutions is lower than that of pure SA solution especially at high HNTs loading (except the SA2N1), which may be related to the formation of filler networks at high nanoparticle loading in the polymer matrix. The decrease trend of the n value was in accord with the polymer-clay (montmorillonite) composite systems [42].

3.2. Structure of SA/HNTs composite hydrogel

FTIR was employed to examine whether there are interfacial interactions between SA and HNTs (Fig. 2(a)). SA exhibits typical peaks of OH stretching band at 3386 cm^{-1}, asymmetric –COO– stretching vibration at 1634 cm^{-1}, and symmetric –COO– stretching vibration at 1419 cm^{-1} [43]. HNTs show characteristic peaks at 3696 and 3624 cm^{-1} attributed to the stretching of hydroxyl groups on their inner and surface [44]. As shown in Fig. 2(b), the peaks at 1419 cm^{-1} shift to higher wavenumbers in the composites (expect SA2N1), which suggests the hydrogen bonds between SA and HNTs. No new peak appears in the FTIR spectrum of the composite hydrogels, which suggests that no chemical reaction occurs between the SA and HNTs. The interfacial interactions are beneficial to the properties enhancement for the composites. The XRD profiles of pure SA dry hydrogel, HNTs, and SA/HNTs composites dry hydrogels are shown in Fig. 2(c). The pure SA shows no distinct peaks due to its amorphous structure [45]. The diffraction peaks of the SA/HNTs composites appear in $2\theta = 12.3°$, 20.1° and 25° assigned to (001), (020, 110), and (020) plane of HNTs respectively [46]. It is should be noted that HNTs powder dope with some kaolinite and quartz [47], there are four peaks of impurity shown in the place of $2\theta = 8.9°$, 18.2°, 30.3°, 35.2°. With the increase in the HNTs loading in the composites, the XRD patterns of composites are much closer to HNTs. When comparing the XRD patterns with that of raw HNTs, no

Table 1
The rheometrical parameters of the power law models.

Samples	SA	SA2N1	SA1N1	SA1N2	SA1N4
k (Pa·s^n)	0.2971	0.4937	0.6517	0.8325	1.2445
n	0.8885	0.9246	0.8859	0.8817	0.7367
R^2	0.9945	0.9847	0.9666	0.9936	0.9769

new diffraction peak appears and the location of the peaks does not change. So the crystal structure of HNTs is retained in the composites.

The SEM images of pure SA and SA/HNTs composite hydrogels were further conducted to characterize the pore structure (Fig. 3(a)). It can be observed that the pore size of the scaffolds is in the range of 100–250 μm. The pore size of 200 μm is suited for cell growth and proliferation [48]. With the increase in HNTs concentration, the roughness of pore surface increases due to the presence of nanosized HNTs. The rough pore walls can provide a good interface for cell adhesion. The pore size of composite hydrogels slightly decreases compared with pure SA hydrogel. Water is porogen in the present hydrogel system. Addition of HNTs into the SA solution leads to the decrease in water content of the same volume hydrogels, which results in the decrease in pore size during the freeze-drying process. The morphology of the freeze-dried SA and SA/HNTs composite hydrogels was further stained with FITC and analyzed by fluorescent microscope (Fig. 3(b)). The results are the same as the SEM images. All the pores are interconnected with pores size of 100 to 250 μm. The pore size slightly decreases with increasing HNTs loading. In total, SEM and fluorescent microscope studies confirmed the 3-D architecture of the hydrogels. The high porosity of the hydrogel can provide a high surface area for cell-materials interactions and sufficient space for extracellular matrix secretion. The pore structure of the hydrogel is beneficial to homogeneous cell seeding and penetration, which will be discussed further below.

3.3. Mechanical properties of the SA/HNTs composite hydrogels

Shrinkage ratio after crosslinking by Ca^{2+} of the different hydrogel samples is compared in Fig. 4(a). Shrinkage ratio is obviously decreased by the addition of HNTs. The shrinkage ratio of SA1N4 is 13%, while it is 31% for pure SA hydrogel. This is attributed to that the addition of HNTs increases the dimensional stability of SA. Also, the stiffness of composite hydrogels increased with HNTs loading from touch of hands. The compressive strength of the different samples was then quantitatively compared in Fig. 4(b). From the strain–stress curve, the compressive properties of composite hydrogels are generally higher than pure SA hydrogel. The SA/HNTs composite hydrogels with 80% HNTs loading exhibit the compressive stress of 2.99 MPa at 80% strain, while the stress at 80% strain of pure SA hydrogel is only 0.8 MPa. So, HNTs can effectively improve the mechanical properties of SA hydrogels. The high reinforcing ability of HNTs towards other polymers was also found [49]. Besides, all the hydrogels can tolerate stain beyond 80% without smash, suggesting the good toughness of the hydrogel. In total, the mechanical properties can meet the requirement of tissue engineering application.

The influence of HNTs on the dynamic viscoelasticity of the composite hydrogels was further studied. The relationships between storage modulus (G′) and strain of the hydrogels are shown in Fig. 4(c). It can be seen that the storage modulus of composite hydrogels increase

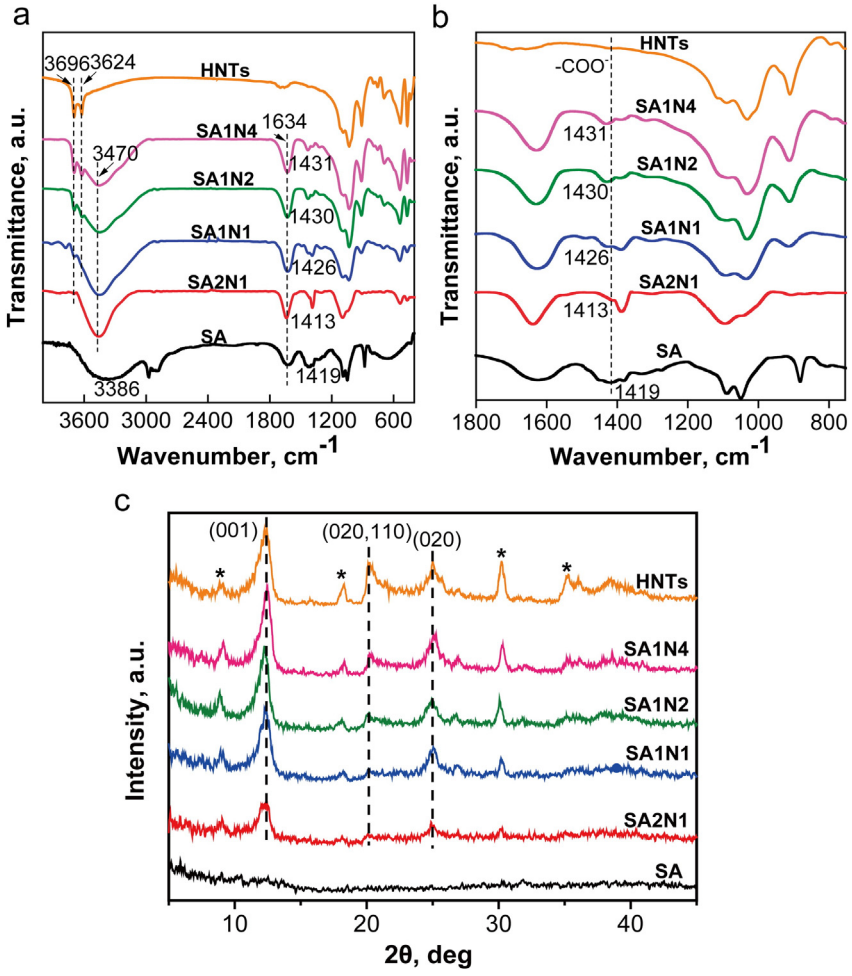

Fig. 2. (a) FTIR spectra of HNTs, SA, and SA/HNTs composites; (b) the FTIR spectra in the range of 1800 to 750 cm^{-1}; (c) XRD pattern of HNTs, SA and SA/HNTs composite (* represent the impurity in HNTs).

with HNTs concentration. For example, the G′ of the SA hydrogel at 0.1% strain is 16,413.0 Pa, while the SA1N4 hydrogel is up to 86,976.2 Pa which is 5.3 folds of that of pure SA hydrogel. The G′ almost keep same from 0.1% to 1% strain for all of the hydrogel samples, but the G′ decreases sharply beyond 1%. This can be explained by that at high strain the crosslink network is destroyed which leads to the decrease of the G′. From the strain sweeping result, HNTs exhibit a significant reinforcing effect on SA hydrogel. Fig. 4(d) further shows G′ curves in frequency sweep for different hydrogels. Consistent with previous result, the addition of HNTs leads to the increase of G′ at low frequency wide (0.1 to ~60 Hz). The G′ of the five hydrogels depends on HNTs loading, and the G′ of pure SA hydrogel is the lowest among all the samples. This can be understood by that HNTs can limit the mobility of macromolecules chains during shear and therefore the composite hydrogels exhibit enhanced modulus. Similar phenomenon was found in other polymer composite hydrogel systems containing HNTs [50,51]. The increasing trend of G′ at high frequency disappears, which is attributed to all the hydrogels exhibit dramatically increased G′ at high frequency.

3.4. Thermal and swelling properties of SA/HNTs composite hydrogels

The DSC thermogram of SA and SA/HNTs composite dried gels is shown in Fig. 5(a). For every curve, an endothermic peak is found at around 116 °C which is attributed to the loss of water correspond to the hydrophilic nature of the functional groups of native alginate [52]. The peak slightly shifts to high temperature and the peak area decreases with the addition of HNTs. For example, the SA1N2 containing 33 wt.% HNTs shows an endothermic peak at 121 °C. This phenomenon is caused by that the loss of water is much less and harder in the composites due to the more compact network. The DSC result also supports the interfacial interactions between the SA and HNTs.

The swelling curves of the SA and composite hydrogels in NaCl solution (0.1 mol/L) are presented in Fig. 5(b). The SA/HNTs composite hydrogels exhibit low swelling ratios with same immersing time compared with pure SA hydrogel. With the increases in HNTs loading, the swelling ratios of the composites gradually decrease. For instance, the swelling ratio of SA1N4 after 80 h is only 1.8, while it is 10.5 for pure SA. The decreased swelling ratio is caused by the decreased hydrophilic polymer content in the composites by the addition of HNTs. In comparison to SA, the water absorption ratio of HNTs is low. In previous studies, a similar decreased swelling ratio of composites by the addition of HNTs was also found [21,51,53].

3.5. Cytocompatibility of SA/HNTs composite hydrogels

A good biocompatibility is the basic requirement of scaffolds employed in tissue engineering. To determine whether the SA/HNTs composite hydrogels are suitable for tissue engineering scaffolds, the cell adhesion and growth behavior were observed. Fig. 6(a) shows the fluorescent microscope images of the MC3T3-E1 cell after 72 h culture on the hydrogel samples. Cells can grow well on the control group (TCPS), indicating the good state of the used cells. In the hydrogel sample, both single cell and cell aggregates are found on the 3D hydrogel. Due to that the cells in the hydrogel are located in different depth, it is hard to focus all the cells in an image. No instinct cell morphology difference can be identified for the SA hydrogel and the composites hydrogel. Among the composite hydrogel, the SA1N1 sample shows much more cell number from the fluorescent microscope images. This may be attributed to the incorporation of proper content of HNTs leads to an increase in the cytocompatibility of SA.

To compare the cell viability for different groups, the extract liquids of the hydrogels were added into the cell culture medium with a ratio of 1:2. Then the mixture solution was added into the cells and the cell viability was detected via the absorbance after 72 h. Fig. 6(b) shows the cell viability determined by MTT method for different group. All the groups show cell viability higher than 85%, suggesting a high cytocompatibility of the hydrogels. Adding an appropriate amount of HNTs can improve the cytocompatibility of SA, since the absorbance value of SA1N2 and

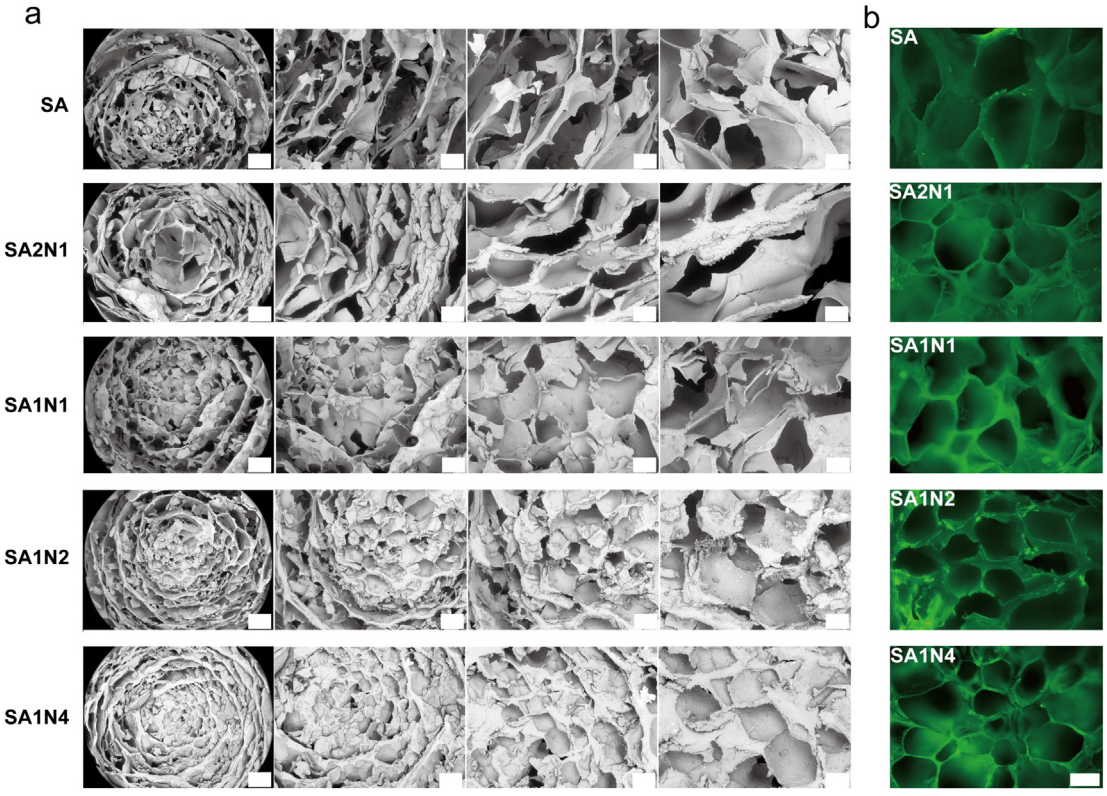

Fig. 3. (a) SEM images of cross section of pure SA and SA/HNTs composite hydrogels. Scale bar: from left, 25× (600 μm), 50× (300 μm), 100× (150 μm) and 200× (75 μm); (b) fluorescent images of cross section of pure SA and SA/HNTs composite hydrogels, which stained with FITC. Scale bar = 100 μm.

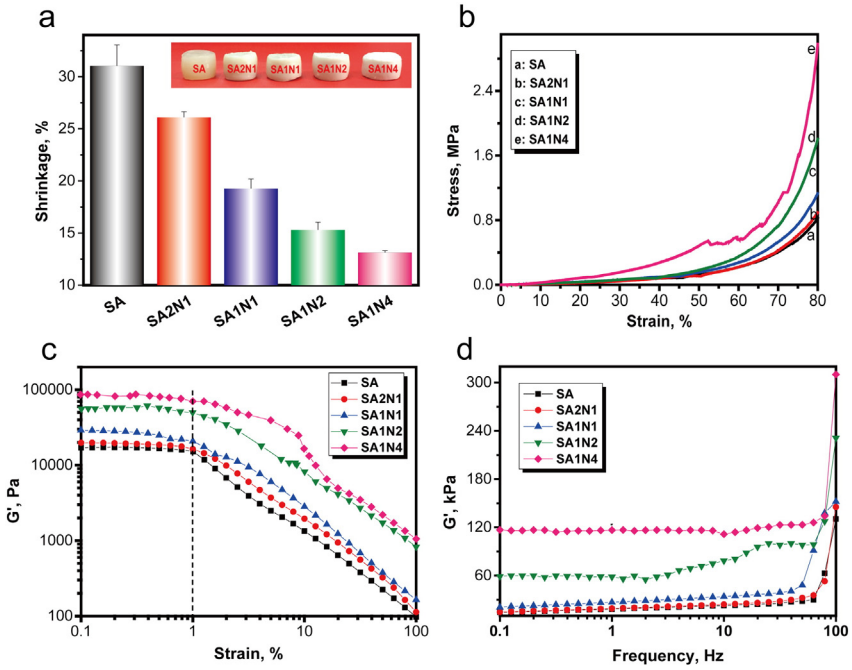

Fig. 4. (a) Shrinkage of SA and SA/HNTs composite hydrogels; (b) compressive stress–strain curves of pure SA and SA/HNTs composite hydrogels; (c) storage modulus vs. strains and frequency of the SA and SA/HNTs composite hydrogels; (d) storage modulus vs. frequency of the SA and SA/HNTs composite hydrogels.

SA1N1 is greater than that of pure SA. However, overloading of HNTs into SA is can leads to the decrease in the MC3T3-E1 cells proliferation. Compared with the control group, SA1N2 and SA1N4 gels are statistically significant ($P < 0.05$). Incorporation of HNTs into polymer can leads to the increase of the cytocompatbility which is attributed the instinct good biocompatibility of HNTs and the increase surface roughness by the nanoparticles [21,24,54,55].

CLSM was further used to characterize the cell morphology on the hydrogels. Fig. 6 (c) shows the CLSM images of cells cultured on SA, SA2N1, and SA1N1 for 3 day. The nuclei and cytoplasm were stained into blue and red color with DAPI and phalloidin-TRITC respectively. Consistent with the fluorescent microscope result, all the hydrogels can support the MC3T3-E1 cells growth. The cells on the composite hydrogel surfaces exhibit diffuse cytoskeleton and well-stretched actin bundle, also the small pseudopodia stretched out obviously with one or more foot processes. In contrast, the cells cultured on pure SA hydrogel show an elongated shape with little thin filopodia and filaments. The total adhesive area of cells cultured on the composite hydrogel surfaces is clearly higher than that of cultured on pure SA hydrogel, suggesting the improved cytocompatibility of the composites. The addition of other nanoparticles also can lead to the improved cytocomaptibiltiy of polymers [56,57].

4. Conclusions

SA/HNTs composite hydrogels were prepared by the method of solution-mixing and subsequent cross-linking with calcium ions. The static and shear viscosity of SA/HNTs solutions increases by the addition of HNTs. The rheological behaviors of pure SA and SA/HNTs solutions fit well with the power law model and showed a shear thinning behavior. Hydrogen bond interactions occur between HNTs and SA as illustrated by FTIR result. The crystal structure of HNTs is retained in the composites. An interconnected pore structure with pore size of 100–250 μm is found in the hydrogels and the addition of HNTs leads to slightly decreased in pore size. The composite hydrogels exhibit a significantly improved in stiffness and compressive strength. The storage modulus of composite hydrogels is greater than that of pure SA hydrogel. The DSC endothermic peak area and swelling ratios of the SA hydrogel decrease by the incorporation of HNTs. SA/HNTs composite hydrogels have low cytotoxicity and show an increase trend in MC3T3-E1 cells adhesion and proliferation compared to the pure SA hydrogel. Together, the advantageous physical properties in combination with the cytocompatibility make the SA/HNTs composite hydrogel scaffolds a promising application in bone tissue engineering.

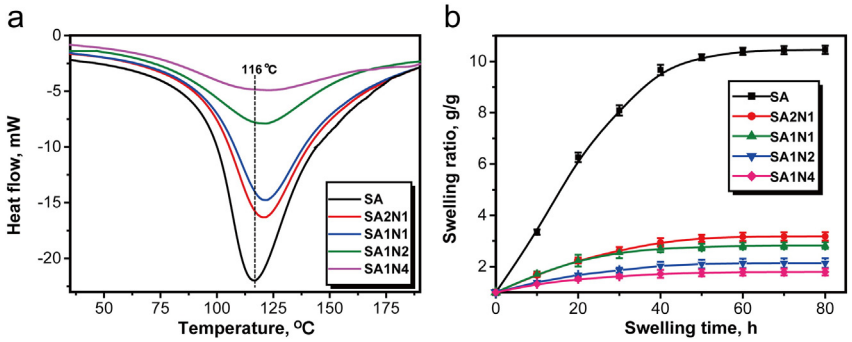

Fig. 5. (a) DSC thermogram for pure SA and SA/HNTs composites; (b) swelling properties of pure SA and SA/HNTs composite hydrogels in 0.1 M NaCl solution at 37 °C.

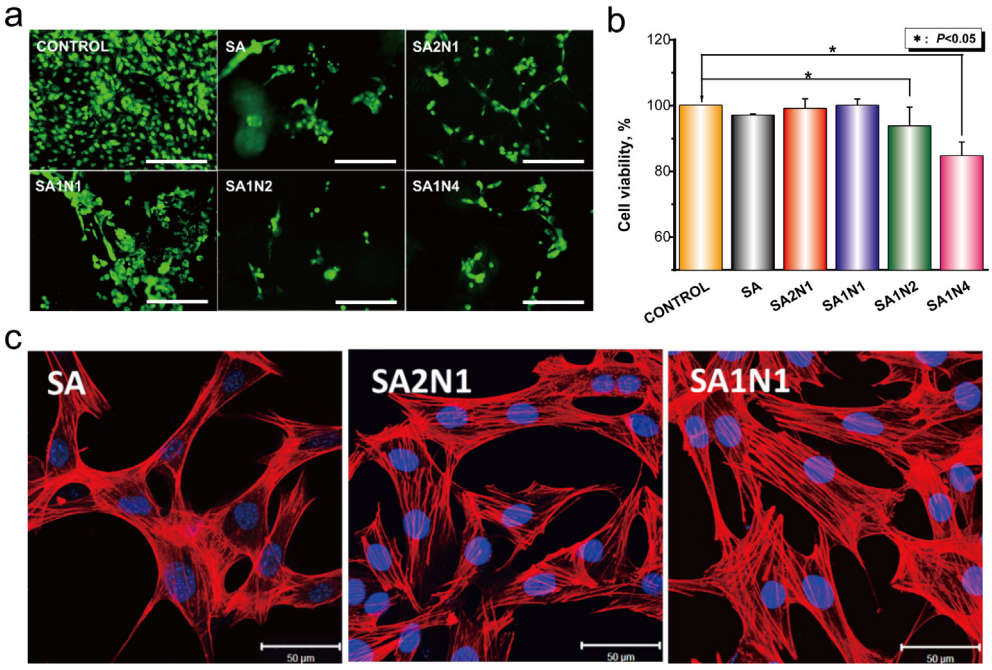

Fig. 6. (a) Fluorescent micrographs of MC3T3-E1 cells postseeding on the SA and SA/HNTs composite hydrogels after 72 h, scale bar = 200 μm; (b) the cell viability of the extracted liquid of the hydrogels determined by MTT assay at 72 h; (c) CLSM micrograph of MC3T3-E1 cells after 72 h cultured on SA, SA2N1, and SA1N1 hydrogels surface, scale bar = 50 μm.

Acknowledgments

This work was financially supported by National High Technology Research and Development Program of China (2015AA020915), the National Natural Science Foundation of China (grant No. 51473069 and 51502113), and the Guangdong Natural Science Funds for Distinguished Young Scholar (grant No. S2013050014606), Science and Technology Planning Project of Guangdong Province (2014A020217006), Guangdong Special Support Program (2014TQ01C127), the Special Fund for Ocean-Scientific Research in the public interest (201405105), and the Pearl River S&T Nova Program of Guangzhou (201610010026).

References

[1] R. Cancedda, P. Giannoni, M. Mastrogiacomo, A tissue engineering approach to bone repair in large animal models and in clinical practice, Biomaterials 28 (2007) 4240–4250.
[2] T. Boontheekul, H.-J. Kong, D.J. Mooney, Controlling alginate gel degradation utilizing partial oxidation and bimodal molecular weight distribution, Biomaterials 26 (2005) 2455–2465.
[3] S. Bose, M. Roy, A. Bandyopadhyay, Recent advances in bone tissue engineering scaffolds, Trends Biotechnol. 30 (2012) 546–554.
[4] S. Bose, S. Tarafder, Calcium phosphate ceramic systems in growth factor and drug delivery for bone tissue engineering: a review, Acta Biomater. 8 (2012) 1401–1421.
[5] S. Yang, K.-F. Leong, Z. Du, C.-K. Chua, The design of scaffolds for use in tissue engineering. part I. traditional factors, Tissue Eng. 7 (2001) 679–689.
[6] X. Liu, J.M. Holzwarth, P.X. Ma, Functionalized synthetic biodegradable polymer scaffolds for tissue engineering, Macromol. Biosci. 12 (2012) 911–919.
[7] N. Iwasaki, S.-T. Yamane, T. Majima, Y. Kasahara, A. Minami, K. Harada, S. Nonaka, N. Maekawa, H. Tamura, S. Tokura, Feasibility of polysaccharide hybrid materials for scaffolds in cartilage tissue engineering: evaluation of chondrocyte adhesion to polyion complex fibers prepared from alginate and chitosan, Biomacromolecules 5 (2004) 828–833.
[8] B.B. Mandal, A. Grinberg, E.S. Gil, B. Panilaitis, D.L. Kaplan, High-strength silk protein scaffolds for bone repair, Proc. Natl. Acad. Sci. 109 (2012) 7699–7704.
[9] J.M. Chupa, A.M. Foster, S.R. Sumner, S.V. Madihally, H.W. Matthew, Vascular cell responses to polysaccharide materials: in vitro and in vivo evaluations, Biomaterials 21 (2000) 2315–2322.
[10] W.R. Gombotz, S.F. Wee, Protein release from alginate matrices, Adv. Drug Deliv. Rev. 64 (2012) 194–205.
[11] S.N. Pawar, K.J. Edgar, Alginate derivatization: a review of chemistry, properties and applications, Biomaterials 33 (2012) 3279–3305.
[12] K.Y. Lee, D.J. Mooney, Alginate: properties and biomedical applications, Prog. Polym. Sci. 37 (2012) 106–126.
[13] J.L. Drury, D.J. Mooney, Hydrogels for tissue engineering: scaffold design variables and applications, Biomaterials 24 (2003) 4337–4351.
[14] H. Tan, K.G. Marra, Injectable, biodegradable hydrogels for tissue engineering applications, Materials 3 (2010) 1746–1767.
[15] Y. Huang, M. Yao, X. Zheng, X. Liang, X. Su, Y. Zhang, A. Lu, L. Zhang, Effects of chitin whiskers on physical properties and osteoblast culture of alginate based nanocomposite hydrogels, Biomacromolecules 16 (2015) 3499–3507.
[16] M. Castilho, J. Rodrigues, I. Pires, B. Gouveia, M. Pereira, C. Moseke, J. Groll, A. Ewald, E. Vorndran, Fabrication of individual alginate-TCP scaffolds for bone tissue engineering by means of powder printing, Biofabrication 7 (2015) 015004.
[17] J. Roosen, J. Pype, K. Binnemans, S. Mullens, Shaping of alginate–silica hybrid materials into microspheres through vibrating-nozzle technology and their use for the recovery of neodymium from aqueous solutions, Ind. Eng. Chem. Res. 54 (2015) 12836–12846.
[18] M. Ionita, M.A. Pandele, H. Iovu, Sodium alginate/graphene oxide composite films with enhanced thermal and mechanical properties, Carbohydr. Polym. 94 (2013) 339–344.
[19] M. Martín-Villena, F. Fernández-Campos, A. Calpena-Campmany, N. Bozal-de Febrer, M. Ruiz-Martínez, B. Clares-Naveros, Novel microparticulate systems for the vaginal delivery of nystatin: development and characterization, Carbohydr. Polym. 94 (2013) 1–11.
[20] Y. He, N. Zhang, Q. Gong, H. Qiu, W. Wang, Y. Liu, J. Gao, Alginate/graphene oxide fibers with enhanced mechanical strength prepared by wet spinning, Carbohydr. Polym. 88 (2012) 1100–1108.
[21] M. Liu, L. Dai, H. Shi, S. Xiong, C. Zhou, In vitro evaluation of alginate/halloysite nanotube composite scaffolds for tissue engineering, Mater. Sci. Eng. C 49 (2015) 700–712.
[22] M. Du, B. Guo, D. Jia, Newly emerging applications of halloysite nanotubes: a review, Polym. Int. 59 (2010) 574–582.
[23] M. Liu, Y. Shen, P. Ao, L. Dai, Z. Liu, C. Zhou, The improvement of hemostatic and wound healing property of chitosan by halloysite nanotubes, RSC Adv. 4 (2014) 23540–23553.
[24] M. Liu, C. Wu, Y. Jiao, S. Xiong, C. Zhou, Chitosan–halloysite nanotubes nanocomposite scaffolds for tissue engineering, J. Mater. Chem. B 1 (2013) 2078–2089.
[25] M. Liu, Y. Zhang, C. Wu, S. Xiong, C. Zhou, Chitosan/halloysite nanotubes bionanocomposites: structure, mechanical properties and biocompatibility, Int. J. Biol. Macromol. 51 (2012) 566–575.
[26] P. Luo, Y. Zhao, B. Zhang, J. Liu, Y. Yang, J. Liu, Study on the adsorption of neutral red from aqueous solution onto halloysite nanotubes, Water Res. 44 (2010) 1489–1497.
[27] Y. Lvov, E. Abdullayev, Functional polymer–clay nanotube composites with sustained release of chemical agents, Prog. Polym. Sci. 38 (2013) 1690–1719.
[28] C. Dionisi, N. Hanafy, C. Nobile, M.L. De Giorgi, R. Rinaldi, S. Casciaro, Y. Lvov, S. Leporatti, Halloysite clay nanotubes as carriers for curcumin: characterization and application, IEEE Trans. Nanotechnol. 2016, http://dx.doi.org/10.1109/TNANO.2016.2524072.
[29] Y.M. Lvov, D.G. Shchukin, H. Mohwald, R.R. Price, Halloysite clay nanotubes for controlled release of protective agents, ACS Nano 2 (2008) 814–820.
[30] K. Ariga, M. McShane, Y.M. Lvov, Q. Ji, J.P. Hill, Layer-by-layer assembly for drug delivery and related applications, Expert Opin. Drug Deliv 8 (2011) 633–644.

[31] K. Ariga, Y.M. Lvov, K. Kawakami, Q. Ji, J.P. Hill, Layer-by-layer self-assembled shells for drug delivery, Adv. Drug Deliv. Rev. 63 (2011) 762–771.
[32] B.T. Greene, A.D. Hughes, M.R. King, Circulating tumor cells: the substrate of personalized medicine? Front. Oncol. 2 (2012) 69.
[33] M. Liu, R. He, J. Yang, W. Zhao, C. Zhou, Stripe-like clay nanotubes patterns in glass capillary tubes for capture of tumor cells, ACS Appl. Mater. Interfaces 8 (2016) 7709–7719.
[34] L. Fan, J. Zhang, A. Wang, In situ generation of sodium alginate/hydroxyapatite/halloysite nanotubes nanocomposite hydrogel beads as drug-controlled release matrices, J. Mater. Chem. B 1 (2013) 6261–6270.
[35] L. Liu, Y. Wan, Y. Xie, R. Zhai, B. Zhang, J. Liu, The removal of dye from aqueous solution using alginate-halloysite nanotube beads, Chem. Eng. J. 187 (2012) 210–216.
[36] G. Cavallaro, A. Gianguzza, G. Lazzara, S. Milioto, D. Piazzese, Alginate gel beads filled with halloysite nanotubes, Appl. Clay Sci. 72 (2013) 132–137.
[37] C. Chang, M. He, J. Zhou, L. Zhang, Swelling behaviors of pH-and salt-responsive cellulose-based hydrogels, Macromolecules 44 (2011) 1642–1648.
[38] C. Zhu, C. Brown, G. Gillies, P. Watkinson, J. Bronlund, Characterizing the rheological properties of mozzarella cheese at shear rate and temperature conditions relevant to pizza baking, LWT Food Sci. Technol. 64 (2015) 82–87.
[39] P. Sopade, T. Filibus, The influence of solid and sugar contents on rheological characteristics of akamu, a semi-liquid maize food, J. Food Eng. 24 (1995) 197–211.
[40] S. Mousazadeh, A. Shakouri, M. Hojjat, S.G. Etemad, S.Z. Heris, Rheological behavior of starch–poly (vinyl alcohol)–TiO_2 nanofluids and their main and interactive effects, J. Appl. Polym. Sci. 133 (2016) 44062.
[41] B. Safadi, R. Andrews, E. Grulke, Multiwalled carbon nanotube polymer composites: synthesis and characterization of thin films, J. Appl. Polym. Sci. 84 (2002) 2660–2669.
[42] F. La Mantia, R. Scaffaro, M. Ceraulo, M. Mistretta, N.T. Dintcheva, L. Botta, A simple method to interpret the rheological behaviour of intercalated polymer nanocomposites, Composites Part B 98 (2016) 382–388.
[43] G. Lawrie, I. Keen, B. Drew, A. Chandler-Temple, L. Rintoul, P. Fredericks, L. Grøndahl, Interactions between alginate and chitosan biopolymers characterized using FTIR and XPS, Biomacromolecules 8 (2007) 2533–2541.
[44] P. Yuan, P.D. Southon, Z. Liu, M.E. Green, J.M. Hook, S.J. Antill, C.J. Kepert, Functionalization of halloysite clay nanotubes by grafting with γ-aminopropyltriethoxysilane, J. Phys. Chem. C 112 (2008) 15742–15751.
[45] T. Tripathy, S. Pandey, N. Karmakar, R. Bhagat, R. Singh, Novel flocculating agent based on sodium alginate and acrylamide, Eur. Polym. J. 35 (1999) 2057–2072.
[46] G. Brindley, K. Robinson, D. MacEwan, The clay minerals halloysite and meta-halloysite, Nature 157 (1946) 225–226.
[47] R. Rong, X. Xu, S. Zhu, B. Li, X. Wang, K. Tang, Facile preparation of homogeneous and length controllable halloysite nanotubes by ultrasonic scission and uniform viscosity centrifugation, Chem. Eng. J. 291 (2016) 20–29.
[48] C.M. Murphy, M.G. Haugh, F.J. O'Brien, The effect of mean pore size on cell attachment, proliferation and migration in collagen–glycosaminoglycan scaffolds for bone tissue engineering, Biomaterials 31 (2010) 461–466.
[49] M. Liu, Z. Jia, D. Jia, C. Zhou, Recent advance in research on halloysite nanotubes-polymer nanocomposite, Prog. Polym. Sci. 39 (2014) 1498–1525.
[50] M. Liu, J. Huang, B. Luo, C. Zhou, Tough and highly stretchable polyacrylamide nanocomposite hydrogels with chitin nanocrystals, Int. J. Biol. Macromol. 78 (2015) 23–31.
[51] M. Liu, W. Li, J. Rong, C. Zhou, Novel polymer nanocomposite hydrogel with natural clay nanotubes, Colloid Polym. Sci. 290 (2012) 895–905.
[52] M. Zohuriaan, F. Shokrolahi, Thermal studies on natural and modified gums, Polym. Test. 23 (2004) 575–579.
[53] M. Liu, Y. Zhang, J. Li, C. Zhou, Chitin-natural clay nanotubes hybrid hydrogel, Int. J. Biol. Macromol. 58 (2013) 23–30.
[54] E. Abdullayev, Y. Lvov, Halloysite clay nanotubes as a ceramic "skeleton" for functional biopolymer composites with sustained drug release, J. Mater. Chem. B 1 (2013) 2894–2903.
[55] H.-Y. Liu, L. Du, Y.-T. Zhao, W.-Q. Tian, In vitro hemocompatibility and cytotoxicity evaluation of halloysite nanotubes for biomedical application, J. Nanomater. 2015 (2015) 685323.
[56] H. Liu, W. Liu, B. Luo, W. Wen, M. Liu, X. Wang, C. Zhou, Electrospun composite nanofiber membrane of poly (l-lactide) and surface grafted chitin whiskers: fabrication, mechanical properties and cytocompatibility, Carbohydr. Polym. 147 (2016) 216–225.
[57] C. Luo, Z. Zou, B. Luo, W. Wen, H. Li, M. Liu, C. Zhou, Enhanced mechanical properties and cytocompatibility of electrospun poly(l-lactide) composite fiber membranes assisted by polydopamine-coated halloysite nanotubes, Appl. Surf. Sci. 369 (2016) 82–91.